Alpha-induced reactions on selenium between 11 and 15 MeV

OPEN ACCESS
IOP Publishing
Journal of Physics G: Nuclear and Particle Physics
J. Phys. G: Nucl. Part. Phys. **44** (2017) 075101 (13pp)
https://doi.org/10.1088/1361-6471/aa7198

Alpha-induced reactions on selenium between 11 and 15 MeV

Stefan Fiebiger[1], Zuzana Slavkovská[1], Ulrich Giesen[2], Kathrin Göbel[1], Tanja Heftrich[1], Annett Heiske[2], René Reifarth[1], Stefan Schmidt[1], Kerstin Sonnabend[1], Benedikt Thomas[1] and Mario Weigand[1]

[1] Institut für Angewandte Physik, Goethe University Frankfurt, Germany
[2] Physikalisch-Technische Bundesanstalt (PTB), Braunschweig, Germany

E-mail: reifarth@physik.uni-frankfurt.de

Received 6 December 2016, revised 20 April 2017
Accepted for publication 8 May 2017
Published 23 May 2017

Abstract

The production of ^{77,79,85,85m}Kr and ^{77}Br via the reaction Se(α, x) was investigated between $E_\alpha = 11$ and 15 MeV using the activation technique. The irradiation of natural selenium targets on aluminum backings was conducted at the Physikalisch-Technische Bundesanstalt (PTB) in Braunschweig, Germany. The spectroscopic analysis of the reaction products was performed using a high-purity germanium detector located at PTB and a low energy photon spectrometer detector at the Goethe University Frankfurt, Germany. Thick-target yields were determined. The corresponding energy-dependent production cross sections of ^{77,79,85,85m}Kr and ^{77}Br were calculated from the thick-target yields. Good agreement between experimental data and theoretical predictions using the TALYS-1.6 code was found.

Keywords: α-induced reactions, activation, γ-spectroscopy

(Some figures may appear in colour only in the online journal)

1. Introduction

Elements heavier than iron are almost exclusively produced in neutron capture processes, the r and s process [1–3]. While many fundamental questions concerning the r process are still unanswered [4], many details of the s process are well known [5]. A part of the s process path

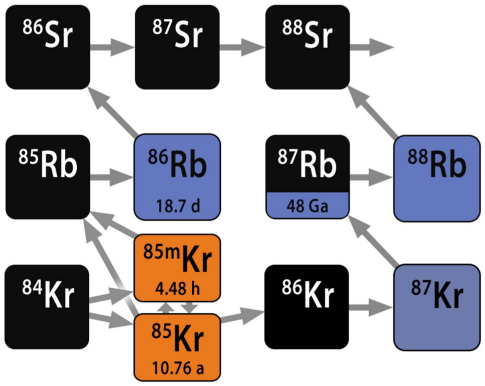

Figure 1. The *s*-process path in the region around the branching point ^{85}Kr. The conditions in the interior of the star are reflected by the branching between neutron capture and β^--decay at ^{85}Kr, which is imprinted in the observable abundance ratio of ^{86}Kr/^{84}Kr. The isomeric state ^{85m}Kr can either populate ^{85}Kr via internal transition or ^{85}Rb via β^--decay. The ground state ^{85}Kr can populate ^{85}Rb via β^--decay, ^{86}Kr neutron capture or, at higher temperatures, ^{85m}Kr via thermal excitation.

and a matter of great interest over the years has been the isotope ^{85}Kr [6]. It represents a branching point in the *s* process because the β-decay rate and the neutron capture rate compete. Therefore the mass flow during the *s* process depends on the stellar conditions during the production, such as temperature and neutron density, see figure 1.

The branching at ^{85}Kr affects the isotopic ratios of the heavy krypton isotopes observed in certain presolar grains, small SiC crystals produced in the outer shells of Red Giants [7]. It was found that the ratio of ^{86}Kr/^{84}Kr exhibits a large scatter, which is probably related to the different conditions at the production site. An explanation of the relation between the observed spread in abundance ratio to the physical conditions inside the star is only possible, if the neutron capture cross section of ^{85}Kr is sufficiently well known [8]. In addition, the idea of using the isobar ^{87}Rb/^{87}Sr to determine the age of the Universe [9, 10] is currently hampered by the insufficient knowledge of the ^{85}Kr(n, γ) cross section [6, 11].

So far, no measurement of the neutron capture cross section of ^{85}Kr in standard kinematics has been performed in the astrophysically interesting keV-regime. The difficulty is that ^{85}Kr is a gaseous radioactive isotope with a half life of $t_{1/2} = 10.8$ yr [12], which sets strict limits on the number of atoms possible inside a γ-calorimeter [13]. We plan to measure the ^{85}Kr(n, γ) cross section in the astrophysically interesting energy region between 1 and 100 keV at the FRANZ facility [14–17]. The production of the necessary material could be achieved by irradiating a sample of ^{82}Se with α-particles [18] and the material could be contained in titanium spheres [19, 20].

Since the corresponding production cross sections are not well known, natural Se was irradiated with α-particles of different energies. The subsequent γ-spectroscopy of the freshly produced radioactive isotopes allowed the determination of production yields for thick targets as well as the determination of cross sections.

2. Sample preparation

In order to fully stop α-particles in the target material, a thick-target layer was produced by melting natural selenium onto an aluminum backing. In total, nine backings with a diameter

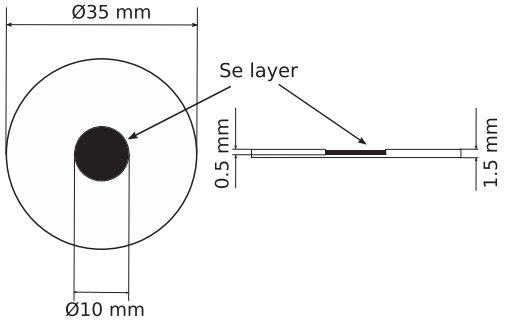

Figure 2. Geometry of the Se backings used for the activation at PTB.

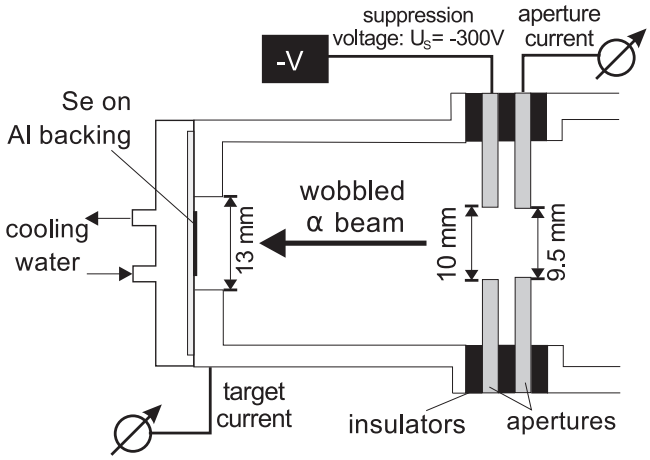

Figure 3. Activation setup of the cyclotron at PTB. A similar setup was already used in previous experiments [25, 26]. Reprinted figure with permission from [25]. Copyright 2011 by the American Physical Society.

of 35 mm, a thickness of 1.5 mm and a recess in the center with a diameter of 10 mm and a depth of 0.5 mm were produced, see figure 2.

The selenium powder was placed in the gap in the center of the backing and heated in an oven to its melting point of 221 °C. Because of the high surface tension of selenium, the liquid selenium formed droplets. To achieve a layer homogeneous enough to stop all incoming α-particles, several steps had to be undertaken. First, the droplets were spread mechanically using a spattle after reducing the oven temperature to approximately 100 °C. Afterwards more selenium powder was put in the gap as a part of it remained on the spattle. The heating procedure was repeated until a smooth glassy black layer of selenium was formed. The resulting thicknesses of the selenium layers were between 240 and 400 μm based on the weight of the samples. This was sufficient for the experiment as the range of alpha particles of 15 MeV in Se is only 100 μm [21].

3. Experiment

The selenium samples were irradiated with α-particles at the cyclotron at PTB [22]. The energy-variable cyclotron provides ion-beam energies up to 27 MeV. For this experiment,

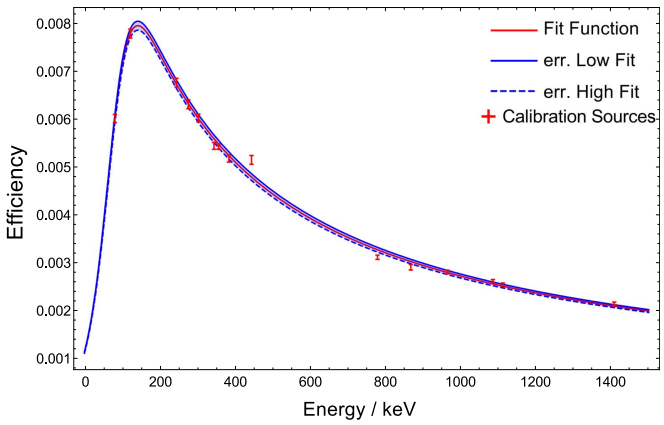

Figure 4. Efficiency of the HPGe detector at PTB Braunschweig.

α-particles with the energies between 11 and 15 MeV were used as the ^{85}Kr production cross section was expected to have a maximum in this energy range [23, 24].

3.1. Irradiation setup

Doubly-charged He ions were extracted from the cyclotron to irradiate the samples in the activation chamber, which is designed as a Faraday cup. A sketch of the chamber is shown in figure 3.

The α-beam was wobbled in order to extent the illumination spot on the samples. The wobbling was optimized for each energy by inserting a quartz window at the target position and checking the illumination. The beam passed three square apertures with increasing edge lengths of 9.5, 10 and 13 mm. The first aperture determined the size of the irradiated area on the target. The targets were placed with the selenium layer facing the beam. Furthermore, the quartz window served as a means to check the dimensions of the beam spot. The maximum dimension of the beam spot in this experiment was 10 mm [25, 26]. This ensured that only the first aperture was actually hit by the α-beam.

For later correction of beam current fluctuations, the collected charge was recorded every 60 s. Secondary electrons were suppressed with a bias voltage of $U_S = -300$ V at the entrance of the activation chamber to ensure a reliable charge measurement. A water cooling system was used in order to reduce the heating of the target, see figure 3.

3.2. Irradiation

First, irradiations to test the thermal stability of Se were performed. Krypton stays trapped in selenium as long as the temperature stays below 50 °C, therefore one requirement for the irradiations was to keep the temperature below this limit [18]. Currents of 4 and 1 μA resulted in Se losses, but a current of 500 nA was found to insure stable production yields of the Kr isotopes and no loss of target material. Five irradiations with activation times between 0.5 and 6.8 h, waiting times between 10 and 45 min and measurement times between 2.5 and 11 h were performed. The first irradiation was performed at an alpha-energy of 13 MeV, the following two at an energy of 11.19 MeV and the last two an energy of 15.1 MeV. All details are summarized in table 1.

Table 1. Beam energy, duration, current and charge of the irradiations.

Run	Beam energy (MeV)	Duration (h)	Average current (nA)	Charge (mC)
1	13	6.8	414	10.08
2	11.19	6.3	472	10.58
3	11.19	6.3	407	9.20
4	15.1	0.5	397	0.71
5	15.1	3.8	405	5.47

Table 2. Measured detection efficiencies of the gammas using the calibration sources ^{152}Eu and ^{133}Ba at the PTB HPGe setup.

Isotope	Energy (keV)	Efficiency (10^{-3})	Isotope	Energy (keV)	Efficiency (10^{-3})
^{152}Eu	121.78	7.79 ± 0.09	^{133}Ba	81.00	6.02 ± 0.09
^{152}Eu	244.7	6.77 ± 0.09	^{133}Ba	276.40	6.32 ± 0.09
^{152}Eu	344.28	5.45 ± 0.07	^{133}Ba	302.85	6.03 ± 0.08
^{152}Eu	443.96	5.16 ± 0.09	^{133}Ba	356.01	5.43 ± 0.06
^{152}Eu	778.91	3.13 ± 0.04	^{133}Ba	383.85	5.19 ± 0.07
^{152}Eu	867.38	2.92 ± 0.06			
^{152}Eu	964.06	2.82 ± 0.04			
^{152}Eu	1085.84	2.62 ± 0.04			
^{152}Eu	1112.08	2.56 ± 0.04			
^{152}Eu	1408.01	2.16 ± 0.03			

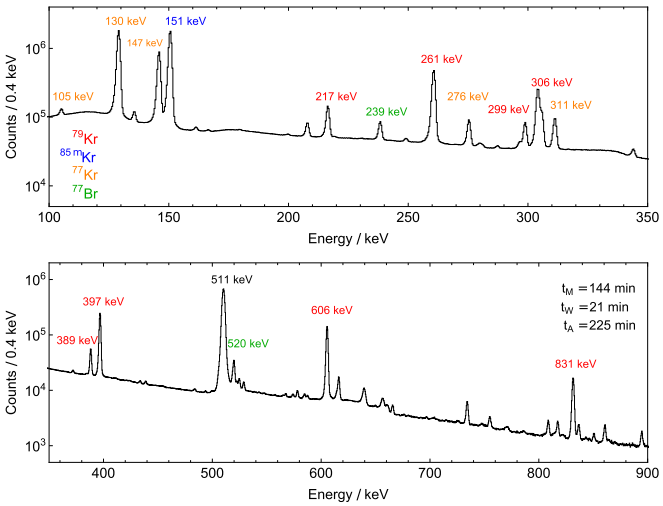

Figure 5. An excerpt from the γ-emission spectrum at the α-energy of 15.1 MeV showing the strongest γ emission lines from ^{77,79,85m}Kr and ^{77}Br used for the determination of α-induced production cross sections.

3.3. Spectroscopic analysis

The spectroscopic analysis of the reaction products ^{77,79,85m}Kr and ^{77}Br was conducted using a high-purity germanium (HPGe) detector at PTB. The dead time was determined using a pulser signal at a frequency of 10 Hz connected to the preamplifier.

Table 3. Gamma emission lines of the examined isotopes with their gamma intensities I_γ, half lives $t_{1/2}$ and efficiencies [12] at the PTB HPGe setup. The only exception is ^{85}Kr, whose activity was determined using the LEPS setup in Frankfurt.

Isotope	Energy (keV)	I_γ (%)	$t_{1/2}$	Efficiency (10^{-3})
^{77}Kr	105.87	1.30 ± 0.09	(74.40 ± 0.60) min	7.36 ± 0.10
^{77}Kr	129.63	81.00 ± 0.2	(74.40 ± 0.60) min	7.90 ± 0.10
^{77}Kr	146.59	37.30 ± 0.19	(74.40 ± 0.60) min	7.95 ± 0.10
^{77}Kr	276.21	2.98 ± 0.18	(74.40 ± 0.60) min	6.33 ± 0.09
^{77}Kr	311.90	3.70 ± 0.50	(74.40 ± 0.60) min	5.92 ± 0.09
^{79}Kr	217.07	2.37 ± 0.13	(35.04 ± 0.10) h	7.12 ± 0.10
^{79}Kr	261.29	12.70 ± 0.40	(35.04 ± 0.10) h	6.51 ± 0.09
^{79}Kr	299.53	1.54 ± 0.09	(35.04 ± 0.10) h	6.06 ± 0.09
^{79}Kr	306.47	2.60 ± 0.13	(35.04 ± 0.10) h	5.98 ± 0.09
^{79}Kr	388.97	1.51 ± 0.09	(35.04 ± 0.10) h	5.21 ± 0.08
^{79}Kr	397.54	9.30 ± 0.40	(35.04 ± 0.10) h	5.14 ± 0.08
^{79}Kr	606.09	8.10 ± 0.30	(35.04 ± 0.10) h	3.19 ± 0.06
^{79}Kr	831.97	1.26 ± 0.07	(35.04 ± 0.10) h	3.13 ± 0.05
^{85m}Kr	151.20	75.20 ± 0.50	(4.480 ± 0.008) h	7.93 ± 0.10
^{85}Kr	514.00	0.43 ± 0.10	(10.74 ± 0.01) y	30.81 ± 0.41
^{77}Br	238.98	23.10 ± 0.50	(57.04 ± 0.12) h	6.81 ± 0.01
^{77}Br	520.69	22.40 ± 0.60	(57.04 ± 0.12) h	4.33 ± 0.07

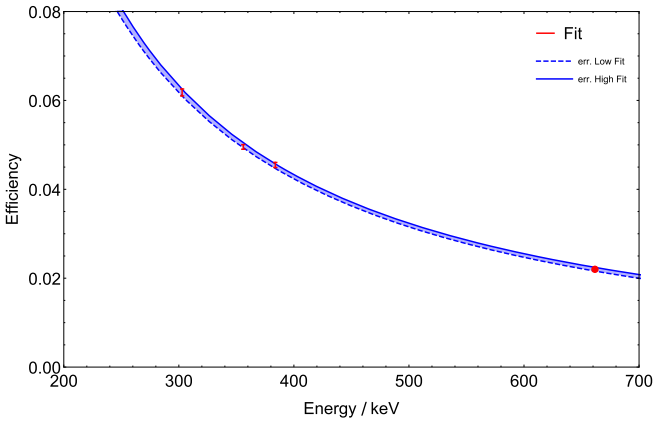

Figure 6. Efficiency of the LEPS detector at the Goethe University Frankfurt.

A phenomenological function f was used to fit the γ-detection efficiencies, which were measured using calibrated sources of ^{152}Eu and ^{133}Ba (figure 4):

$$f(E) = a \cdot \exp[-b \cdot \ln(E - c + d \cdot \exp(e \cdot E))]. \quad (1)$$

All calculated efficiencies are summarized in tables 2 and 3. Figure 5 shows a typical example of a measured spectrum for an α-energy of 15.1 MeV (Run 5, table 1).

Because of the long half life of the ^{85}Kr ground state and the small intensity of its strongest γ-emission line at 514 keV, it was not possible to use the HPGe detector at PTB for its spectroscopic analysis. Therefore, the activity of ^{85}Kr was measured at Goethe University Frankfurt using a low energy photon spectrometer, which has the advantage of a very good

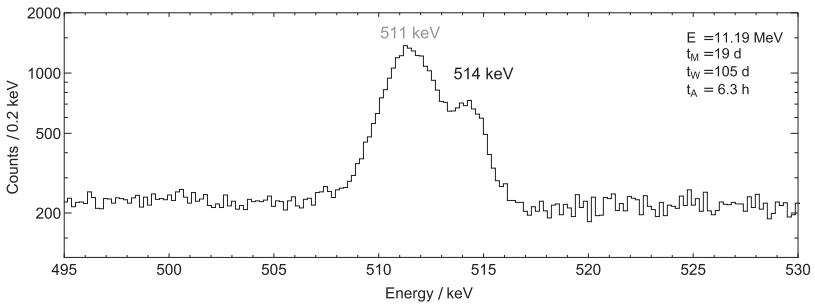

Figure 7. The 514 keV γ-emission line of the ^{85}Kr ground state.

energy resolution and a reasonably large efficiency, figure 6. This allows the separation of the 514 keV γ-line following the decay of $^{85}\mathrm{Kr}^{\mathrm{GS}}$ from the 511 keV background (figure 7).

4. Thick-target yields

This experiment was performed using thick targets. This means that the α-particles were stopped or at least slowed down below the reaction threshold within the selenium layer. Therefore the first quantity that can be derived is the thick-target yield for different beam energies $Y(E)$ in units of reactions per projectile. Energy-dependent cross sections $\sigma(E)$ can then be derived in a second step. The average production rate of a given isotope is

$$R = Y\frac{N_{\mathrm{projectile}}}{t_{\mathrm{A}}}, \tag{2}$$

where $N_{\mathrm{projectile}}$ is the number of α-particles hitting the thick target and t_{A} the irradiation (activation) time. Furthermore, the number of events in the detector corresponding to a γ-energy E_γ is given by

$$C(E_\gamma) = I_\gamma(E_\gamma)\,\epsilon(E_\gamma)\frac{\tau}{t_M}\int_{t_W}^{t_W+t_M} \lambda\, N^{\mathrm{product}}(t)\mathrm{d}t, \tag{3}$$

with $I_\gamma(E_\gamma)$ denoting the γ-intensity, $\epsilon(E_\gamma)$ the detection efficiency, τ the detector life time, λ the decay constant of the investigated isotope, $N^{\mathrm{product}}(t)$ the remaining number of produced nuclei. The waiting time between the end of the activation and the beginning of the γ-counting is given by t_W and t_M the γ-counting time.

Assuming a constant production rate R during the activation, the number of product nuclei follows:

$$\frac{\mathrm{d}N^{\mathrm{product}}}{\mathrm{d}t} = -\lambda\, N^{\mathrm{product}}(t) + R, \tag{4}$$

with the solution

$$N^{\mathrm{product}}(t) = \left(\frac{YN_{\mathrm{projectile}}}{t_{\mathrm{A}}\lambda}(1 - \mathrm{e}^{-\lambda t_{\mathrm{A}}})\right)\mathrm{e}^{-\lambda t}, \tag{5}$$

hence the thick-target yield Y can be written as

$$Y = \frac{C}{I_\gamma\,\epsilon}\frac{t_M}{\tau}\frac{1}{(1 - \mathrm{e}^{-\lambda t_M})\mathrm{e}^{-\lambda t_W}}\frac{\lambda t_{\mathrm{A}}}{1 - \mathrm{e}^{-\lambda t_{\mathrm{A}}}}\frac{1}{N_{\mathrm{projectile}}}. \tag{6}$$

Depending on the investigated isotope, feeding from other decaying isotopes has to be taken into account. In this experiment, ^{77}Kr(EC) feeds ^{77}Br and ^{85m}Kr(IT) feeds its ground state ^{85}Kr. To include the feeding, equation (4) has to be extended:

$$\frac{\mathrm{d}N^{\mathrm{product}}}{\mathrm{d}t} = -\lambda N^{\mathrm{product}}(t) + R + r\lambda_{\mathrm{feed}}N_{\mathrm{feed}}(t), \tag{7}$$

where the index *feed* denotes the decay constant λ and r the branching ratio for decays of the feeding isotope to the examined isotope. The derived thick-target yields for α-particles on natural selenium are summarized in table 4 for the radioactive isotopes ^{77,79,85m,85}Kr and ^{77}Br.

In principle, ^{85}Kr can also be produced via

$$^{82}\mathrm{Se}(\alpha, \mathrm{p})^{85}\mathrm{Br}(\beta^-)^{85}\mathrm{Kr}. \tag{8}$$

^{85}Br has a β^--decay half life time of just $t_{1/2} = 2.90$ min. Consequently it was not possible to disentangle the (α, p) and (α, n) reaction channels based on the data from this experiment because of the long irradiation and simultaneously long waiting times during this experiment. Since the Q-value of the (α, p)-channel is about 2 MeV higher than the Q-value of the (α, n)-channel, the (α, n)-channel is always at least one order of magnitude stronger than the (α, p)-channel. A TALYS-1.6 calculation was performed to verify this observation (see figure 8). Up to an energy of 13 MeV the (α, n)-channel is more than two orders of magnitude stronger than the (α, p)-channel, which is negligible compared to all other uncertainties of this experiment. However, at 15 MeV, a contribution of up to 10% is expected. This branching ratio was consistently observed within the models using a variety of alpha optical potentials and level densities in the TALYS-1.6 calculations. It is worthwhile emphasizing again, that this experiment was a thick-target experiment, which means all energies below the beam energy contributed to the total yield. This contribution is only relevant for the ^{82}Se (α, n)^{85m}Kr, since the decay of ^{85}Br populates almost exclusively (>99%) the isomer ^{85m}Kr [12]. In order to account for a possible contribution of the (α, p)-channel, we included an additional asymmetric uncertainty of 10% for the production yield of ^{85m}Kr at 15.1 MeV. The (α, p)-channel was neglected for all other energies as well as for the ground state production.

5. Integral cross sections

The relation between differential cross sections and thick-target yields is given by:

$$Y(E) = \int_{E_{\mathrm{threshold}}}^{E} \frac{\sigma(E')n_{\mathrm{V,target}}}{S(E')}\mathrm{d}E' \tag{9}$$

($S(E')$ is the stopping power) or in its equivalent differential form:

$$\sigma(E) = \frac{S(E)}{n_{\mathrm{V}}}\frac{\mathrm{d}Y(E')}{\mathrm{d}E'}. \tag{10}$$

To determine an integral cross section from the thick-target yields (see section 4) the following equation can be used

$$\sigma_{\mathrm{integral}}(E) = \frac{Y(E_1) - Y(E_2)}{d \cdot n_{\mathrm{V,target}} \cdot a}, \tag{11}$$

where $E = (E_1 + E_2)/2$, $n_{\mathrm{V,target}}$ is the number of target atoms per unit volume, a is the fraction of the respective selenium isotope and d is the path length of an alpha particle, while it is slowed from E_1 to E_2 based on SRIM [21]. The results for the cross sections including the

Table 4. Thick-target yields of ^{77,79,85,85m}Kr and ^{77}Br for α-particles on natural selenium at the three alpha-energies together with statistical and systematic uncertainties.

E_α	11.19 MeV	13 MeV	15.1 MeV
Isotope	$Y \pm dY_{stat} \pm dY_{syst}$	$Y \pm dY_{stat} \pm dY_{syst}$	$Y \pm dY_{stat} \pm dY_{syst}$
^{77}Kr	$(3.30 \pm 0.14 \pm 0.12)10^{-8}$	$(1.25 \pm 0.10 \pm 0.04)10^{-7}$	$(3.95 \pm 0.10 \pm 0.06)10^{-7}$
^{79}Kr	$(4.09 \pm 0.04 \pm 0.05)10^{-7}$	$(1.89 \pm 0.02 \pm 0.02)10^{-6}$	$(4.52 \pm 0.11 \pm 0.05)10^{-6}$
^{85m}Kr	$(1.77 \pm 0.04 \pm 0.12)10^{-7}$	$(3.72 \pm 0.09 \pm 0.25)10^{-7}$	$(4.68 \pm 0.11 + 0.32 - 0.57)10^{-7}$
^{85}Kr	$(1.99 \pm 0.11 \pm 0.13)10^{-7}$	$(8.48 \pm 0.30 \pm 0.43)10^{-7}$	$(1.33 \pm 0.04 \pm 0.06)10^{-6}$
^{77}Br	$(3.76 \pm 0.12 \pm 0.19)10^{-9}$	$(3.78 \pm 0.18 \pm 0.21)10^{-8}$	$(1.14 \pm 0.02 \pm 0.06)10^{-7}$

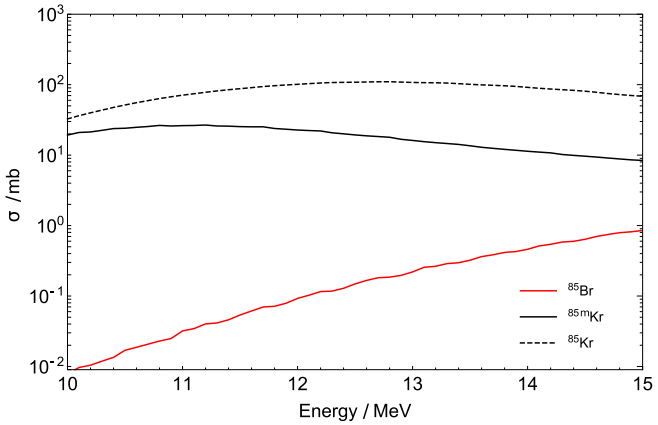

Figure 8. Comparison of the theoretical production cross sections ^{82}Se(α, p)^{85}Br, ^{82}Se (α, n)^{85}Kr and ^{82}Se(α, n)^{85m}Kr computed with TALYS-1.6 using the default input parameters.

Table 5. Alpha-induced production cross sections of ^{77,79,85,85m}Kr and ^{77}Br at the alpha-energies of 11..13 and 13..15 MeV with statistical and systematic uncertainties.

E_α	11..13 MeV	13..15 MeV
Reaction	σ (mb)	σ (mb)
^{74}Se(α, n)^{77}Kr	$164.1 \pm 5.1_{\text{stat}} \pm 14.5_{\text{syst}}$	$414.2 \pm 13.0_{\text{stat}} \pm 34.1_{\text{syst}}$
^{76}Se(α, n)^{79}Kr	$247.2 \pm 2.8_{\text{stat}} \pm 14.7_{\text{syst}}$	$397.6 \pm 17.8_{\text{stat}} \pm 24.0_{\text{syst}}$
^{82}Se(α, n)^{85m}Kr	$37.5 \pm 1.4_{\text{stat}} \pm 3.4_{\text{syst}}$	$16.9 \pm 2.2_{\text{stat}} + 1.5_{\text{syst}} - 2.3_{\text{syst}}$
^{82}Se(α, n)^{85}Kr	$124.6 \pm 6.1_{\text{stat}} \pm 16.4_{\text{syst}}$	$84.3 \pm 8.5_{\text{stat}} \pm 11.1_{\text{syst}}$
^{74}Se(α, p)^{77}Br	$62.0 \pm 4.0_{\text{stat}} \pm 5.0_{\text{syst}}$	$122.9 \pm 7.2_{\text{stat}} \pm 9.7_{\text{syst}}$

corresponding energy range $E \pm (E_2 - E_1)/2$ are listed in table 5. This apporach is useful for an easier comparison with differential data.

6. Uncertainty calculation and discussion

The uncertainties of C, E_γ, τ, $N(t)$, t_W, t_M, t_A, and $N_{\text{projectile}}$, were propagated to the final results. First, a weighted average over the count rates of the same γ-line for different runs at the same α-beam energy was calculated and then a weighted average for the yields of all individual γ-lines was computed. The remaining parameters $I_\gamma(E_\gamma)$, $\epsilon(E_\gamma)$ and λ are common between the different runs and were, therefore, considered only after the averaging step. In the case of ^{85m}Kr an additional uncertainty of 10% for the highest energies of the thick-target yield as well as the cross section was implemented as described in section 4. Furthermore, for the cross section calculation (equation (11)) an uncertainty of 5% for the path length d was assumed, the uncertainty of the fraction of selenium isotope a was taken from [27]. This uncertainty was used again for the number of target atoms for the specific isotope $n_{\text{V,target}}$ as it was derived from the selenium density. Summing and pile-up effects were estimated to be smaller than 1% and could therefore be neglected compared to other systematic uncertainties.

Table 6. Comparison of the integral cross section measurements with theoretical estimates from TALYS-1.6 and NON-SMOKER (not available for production of ^{77}Br and ^{85m}Kr) between 11 and 13 MeV. The energy spread of 2 MeV indicates the range of energies contributing the integral cross section determination resulting from the subtraction of two thick-target yields. It does not correspond to 1σ of a Gaussian distribution. The theoretical values result from folding the differential cross section with the energy distribution of the ions in the sample, see equation (12).

Reaction	Experiment	TALYS-1.6	NON-SMOKER
Isotope	$\sigma_{11\,..\,13}$ (mb)	$\sigma_{11..13}$ (mb)	$\sigma_{11..13}$ (mb)
^{74}Se(α, n)^{77}Kr	164 ± 15	159	286
^{76}Se(α, n)^{79}Kr	247 ± 15	244	389
^{82}Se(α, n)^{85m}Kr	37.5 ± 3.8	22.3	—
^{82}Se(α, n)^{85}Kr	124 ± 17	120	431
^{74}Se(α, p)^{77}Br	62.0 ± 6.4	83.7	99.3

Table 7. Comparison of the integral cross section measurements with theoretical estimates from TALYS-1.6 and NON-SMOKER (not available for production of ^{77}Br and ^{85m}Kr) between 13 and 15 MeV. The energy spread of 2 MeV indicates the range of energies contributing the integral cross section determination resulting from the subtraction of two thick-target yields. It does not correspond to 1σ of a Gaussian distribution. The theoretical values result from folding the differential cross section with the energy distribution of the ions in the sample, see equation (12).

Isotope	Experiment	TALYS-1.6	NON-SMOKER
Reaction	$\sigma_{13\,..\,15}$ (mb)	$\sigma_{13\,..\,15}$ (mb)	$\sigma_{13\,..\,15}$ (mb)
^{74}Se(α, n)^{77}Kr	414 ± 36	310	467
^{76}Se(α, n)^{79}Kr	397 ± 30	470	620
^{82}Se(α, n)^{85m}Kr	16.9 ± 3.2	11.6	—
^{82}Se(α, n)^{85}Kr	84 ± 14	102	682
^{74}Se(α, p)^{77}Br	122 ± 12	173	168

Tables 6 and 7 show a comparison of our data with theoretical values calculated with NON-SMOKER [23] and TALYS-1.6 [24]. In order to compare our integral data with the theoretical differential data, the differential data were folded with the energy distribution in the selenium target resulting from the energy loss due to ionization processes:

$$\sigma_{\text{integral}} = \frac{\int_{E_{\min}}^{E_{\max}} \frac{\sigma(E)}{S(E)} \mathrm{d}E}{\int_{E_{\min}}^{E_{\max}} \frac{\mathrm{d}E}{S(E)}}. \tag{12}$$

Previous experimental data for energies between 10 and 15 MeV are only available for the reaction ^{76}Se(α, n)^{79}Kr [28]. These are differential data with large gaps. A direct comparison with our integral data is therefore not possible, but the data agree in general. No other experimental data are available so far. However, we found a generally good agreement between the TALYS-1.6 predictions and our results. The deviations are typically less than 2σ. The deviations from NON-SMOKER predictions are typically larger. In particular in the case of ^{82}Se(α, n) the predicted values from NON-SMOKER are a factor of 3–10 higher than our measurements.

7. Summary

In this experiment, thick-target yields and alpha-induced production cross sections of ^{77,79,85,85m}Kr and ^{77}Br between the alpha-energies of 11 and 15 MeV have been determined via activation technique. The corresponding energy-dependent production cross sections of ^{77,79,85,85m}Kr and ^{77}Br were calculated from the thick-target yields. Good agreement between experimental data and theoretical predictions from TALYS-1.6 was found. The comparison with the NON-SMOKER code yield typically good agreement, except for the case of ^{82}Se(α, n) where a striking difference of a factor of 3–10 was observed.

Acknowledgments

We would like to thank the accelerator crew at PTB as well as the IAP workshop for their support during this project. This project was supported by the European Research Council under the European Union's Seventh Framework Programme (FP/2007–2013)/ERC Grant Agreement n. 615126, HIC for FAIR and NAVI.

References

[1] Wallerstein G *et al* 1997 *Rev. Mod. Phys.* **69** 995–1084
[2] Reifarth R, Lederer C and Käppeler F 2014 *J. Phys. G: Nucl. Part. Phys.* **41** 053101
[3] Pignatari M, Göbel K, Reifarth R and Travaglio C 2016 *Int. J. Mod. Phys.* E **25** 1630003
[4] Arcones A and Thielemann F K 2013 *J. Phys. G: Nucl. Part. Phys.* **40** 013201
[5] Lugaro M, Herwig F, Lattanzio J C, Gallino R and Straniero O 2003 *Astrophys. J.* **586** 1305
[6] Raut R *et al* 2013 *Phys. Rev. Lett.* **111** 112501
[7] Pignatari M, Gallino R, Amari S and Davis A M 2006 *Mem. Soc. Astron. Ital.* **77** 897
[8] Koloczek A, Thomas B, Glorius J, Plag R, Pignatari M, Reifarth R, Ritter C, Schmidt S and Sonnabend K 2016 *At. Data Nucl. Data Tables* **108** 1–14
[9] Beer H and Penzhorn R D 1984 *Astrophys. Space Sci.* **100** 234
[10] Beer H and Walter G 1984 *Astrophys. Space Sci.* **100** 243–53
[11] Bao Z Y, Beer H, Käppeler F, Voss F, Wisshak K and Rauscher T 2000 *At. Data Nucl. Data Tables* **76** 70
[12] Singh B and Chen J 2014 *Nucl. Data Sheets* **116** 1–162
[13] Couture A and Reifarth R 2007 *At. Data Nucl. Data Tables* **93** 807
[14] Reifarth R *et al* 2017 *J. Phys.: Conf. Ser.* accepted
[15] Reifarth R, Haight R C, Heil M, Käppeler F and Vieira D J 2004 *Nucl. Instrum. Methods* A **524** 215
[16] Reifarth R, Chau L P, Heil M, Käppeler F, Meusel O, Plag R, Ratzinger U, Schempp A and Volk K 2009 *Publ. Astron. Soc. Aust.* **26** 255
[17] Wiesner C *et al* 2010 *AIP Conf. Proc.* **1265** 487–92
[18] Suzuki K, Blessing G, Qaim S and Stöcklin G 1982 *Int. J. Appl. Radiat. Isotopes* **33** 1445–8
[19] Rupp G, Petrich D, Käppeler F, Kaltenbaek J, Leugers B and Reifarth R 2009 *Nucl. Instrum. Methods* A **608** 152
[20] Reifarth R, Heil M, Käppeler F, Voss F, Wisshak K, Bečvář F, Krtička M, Gallino R and Nagai Y 2002 *Phys. Rev.* C **66** 064603
[21] Ziegler J 1980 *Handbook of Stopping Cross-section for Energetic Ions in all Elements* vol 5 (New York: Pergamon)
[22] Brede H J, Cosack M, Dietze G, Gumpert H, Guldbakke S, Jahr R, Kutscha M, Schlegel-Bickmann D and Schölermann H 1980 *Nucl. Instrum. Methods* **169** 349–58
[23] Rauscher T and Thielemann F K 2001 *At. Data Nucl. Data Tables* **79** 47

[24] Koning A J, Hilaire S and Duijvestijn M C 2005 Comprehensive nuclear reaction modeling *Int. Conf. on Nuclear Data for Science and Technology* (*American Institute of Physics Conference Series* vol 769) ed R C Haight *et al* (New York: AIP) pp 1154–9
[25] Sauerwein A *et al* 2011 *Phys. Rev.* C **84** 045808
[26] Netterdon L, Demetriou P, Endres J, Giesen U, Kiss G G, Sauerwein A, Szücs T, Zell K O and Zilges A 2013 *Nucl. Phys.* A **916** 149–67
[27] Wang M, Audi G, Wapstra A H, Kondev F G, MacCormick M, Xu X and Pfeiffer B 2012 *Chin. Phys.* C **36** 1603–2014
[28] Levkovskij V N 1991 Activation Cross section by Protons and Alphas (Moscow) EXFOR A0510